A Specific PfEMP1 Is Expressed in P. falciparum Sporozoites and Plays a Role in Hepatocyte Infection

Gigliola Zanghì, Shruthi S. Vembar, Sebastian Baumgarten, Shuai Ding, Julien Guizetti, Jessica Bryant, Denise Mattei, Anja T.R. Jensen, Laurent Rénia, Yun Shan Goh, et al.

Article

Cell Reports

A Specific PfEMP1 Is Expressed in *P. falciparum* Sporozoites and Plays a Role in Hepatocyte Infection

Graphical Abstract

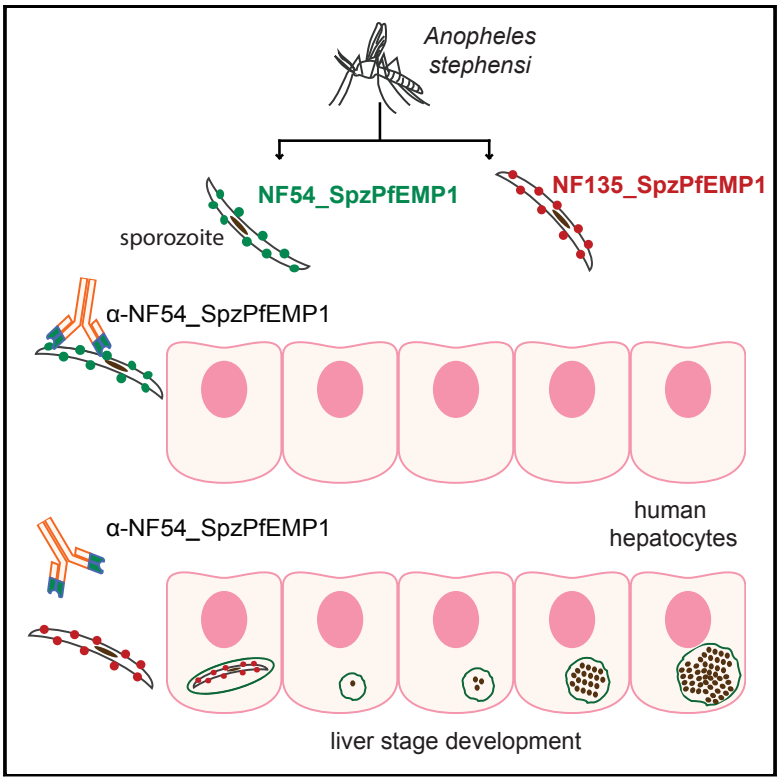

Highlights

- Sporozoites expand subtelomeric heterochromatin to silence blood-stage-specific genes
- A strain-specific PfEMP1 is expressed on the surface of sporozoites
- NF54_SpzPfEMP1 is immunogenic in sporozoite-infected human volunteers
- Antibodies against NF54_SpzPfEMP1 block sporozoite infection of hepatocytes

Authors

Gigliola Zanghì, Shruthi S. Vembar, Sebastian Baumgarten, ..., Salah Mecheri, Dominique Mazier, Artur Scherf

Correspondence

dominique.mazier@upmc.fr (D.M.), artur.scherf@pasteur.fr (A.S.)

In Brief

P. falciparum PfEMP1 surface adhesion proteins mediate immune evasion and pathogenesis during asexual blood stage development. Zanghì et al. find that a strain-specific member of PfEMP1 is expressed at the sporozoite surface. Antibodies against this protein inhibit sporozoite invasion of hepatocytes in a strain-specific manner.

Zanghì et al., 2018, Cell Reports *22*, 2951–2963
March 13, 2018
https://doi.org/10.1016/j.celrep.2018.02.075

CellPress

Cell Reports
Article

A Specific PfEMP1 Is Expressed in *P. falciparum* Sporozoites and Plays a Role in Hepatocyte Infection

Gigliola Zanghì,[1,2,3,4,5,12] Shruthi S. Vembar,[3,4,5] Sebastian Baumgarten,[3,4,5] Shuai Ding,[3,4,5] Julien Guizetti,[3,4,5] Jessica M. Bryant,[3,4,5] Denise Mattei,[3,4,5] Anja T.R. Jensen,[6,7] Laurent Rénia,[8,9] Yun Shan Goh,[8] Robert Sauerwein,[10] Cornelus C. Hermsen,[10] Jean-François Franetich,[1,2,12] Mallaury Bordessoulles,[1,2,12] Olivier Silvie,[1,2,12] Valérie Soulard,[1,2,12] Olivier Scatton,[11] Patty Chen,[3,4,5] Salah Mecheri,[3,4,5] Dominique Mazier,[1,2,12,*] and Artur Scherf[3,4,5,13,*]

[1]Sorbonne Universités, Université Pierre et Marie Curie-Paris 6, UMR S945, 75003 Paris, France
[2]Institut National de la Santé et de la Recherche Médicale, U945, 75013 Paris, France
[3]Unité Biologie des Interactions Hôte-Parasite, Département de Parasites et Insectes Vecteurs, Institut Pasteur, 75015 Paris, France
[4]CNRS, ERL 9195, 75015 Paris, France
[5]INSERM, Unit U1201, 75015 Paris, France
[6]Centre for Medical Parasitology, Department of Immunology & Microbiology, Faculty of Health and Medical Sciences, University of Copenhagen, Copenhagen, Denmark
[7]Department of Infectious Diseases, Copenhagen University Hospital (Rigshospitalet), 2100 Copenhagen, Denmark
[8]Laboratory of Pathogen Immunobiology, Singapore Immunology Network (SIgN), Agency for Science, Technology and Research (A*STAR), Biopolis, Singapore
[9]Department of Microbiology and Immunology, Yong Loo Lin School of Medicine, National University of Singapore, Singapore
[10]Department of Medical Microbiology and Radboud Center for Infectious Diseases, Radboud University Medical Center, P.O. Box 9101, 6500 HB, Nijmegen, the Netherlands
[11]Service de Chirurgie Digestive, Hépato-Bilio-Pancréatique et Transplantation Hépatique, Hôpital Pitié-Salpêtrière, 75013 Paris, France
[12]AP-HP, Groupe Hospitalier Pitié-Salpêtrière, Service de Parasitologie Mycologie, Paris 75013, France
[13]Lead Contact
*Correspondence: dominique.mazier@upmc.fr (D.M.), artur.scherf@pasteur.fr (A.S.)
https://doi.org/10.1016/j.celrep.2018.02.075

SUMMARY

Heterochromatin plays a central role in the process of immune evasion, pathogenesis, and transmission of the malaria parasite *Plasmodium falciparum* during blood stage infection. Here, we use ChIP sequencing to demonstrate that sporozoites from mosquito salivary glands expand heterochromatin at subtelomeric regions to silence blood-stage-specific genes. Our data also revealed that heterochromatin enrichment is predictive of the transcription status of clonally variant genes members that mediate cytoadhesion in blood stage parasites. A specific member (here called NF54*var*^{sporo}) of the *var* gene family remains euchromatic, and the resultant PfEMP1 (NF54_SpzPfEMP1) is expressed at the sporozoite surface. NF54_SpzPfEMP1-specific antibodies efficiently block hepatocyte infection in a strain-specific manner. Furthermore, human volunteers immunized with infective sporozoites developed antibodies against NF54_SpzPfEMP1. Overall, we show that the epigenetic signature of *var* genes is reset in mosquito stages. Moreover, the identification of a strain-specific sporozoite PfEMP1 is highly relevant for vaccine design based on sporozoites.

INTRODUCTION

The most devastating form of human malaria is caused by the protozoan parasite *P. falciparum*, with more than 200 million people infected annually and an estimated 445,000 deaths in 2017 (World Health Organization, 2017). Malaria is transmitted by the bite of an infected *Anopheles* mosquito, which harbors sporozoites in its salivary glands. From the point of injection into the skin, sporozoites migrate via blood vessels to the liver, cross the sinusoidal cell layer separating the blood and the liver, and finally invade hepatocytes where asexual reproduction leads to the release of thousands of merozoites into the bloodstream (Prudêncio and Mota, 2007). Merozoites infect mature red blood cells and, through asexual reproduction, generate daughter merozoites to initiate a new infective cycle. The persistence and pathogenesis of *P. falciparum* during blood stage proliferation relies on the exclusive and successive expression of variant surface adhesion molecules, PfEMP1, expressed at the membranes of infected red blood cells (iRBCs) and mediate cytoadhesion in the microvasculature (Smith, 2014). This immune evasion mechanism, termed "antigenic variation," depends on monoallelic expression of one of approximately 60 *var* genes that encode PfEMP1 proteins.

Different epigenetic factors lead to the default transcriptional silencing of all but one *var* gene via the establishment of facultative heterochromatin (Guizetti and Scherf, 2013). Heterochromatin protein 1 (PfHP1) is a key regulator of facultative heterochromatin in *P. falciparum* (Flueck et al., 2009; Pérez-Toledo et al., 2009),

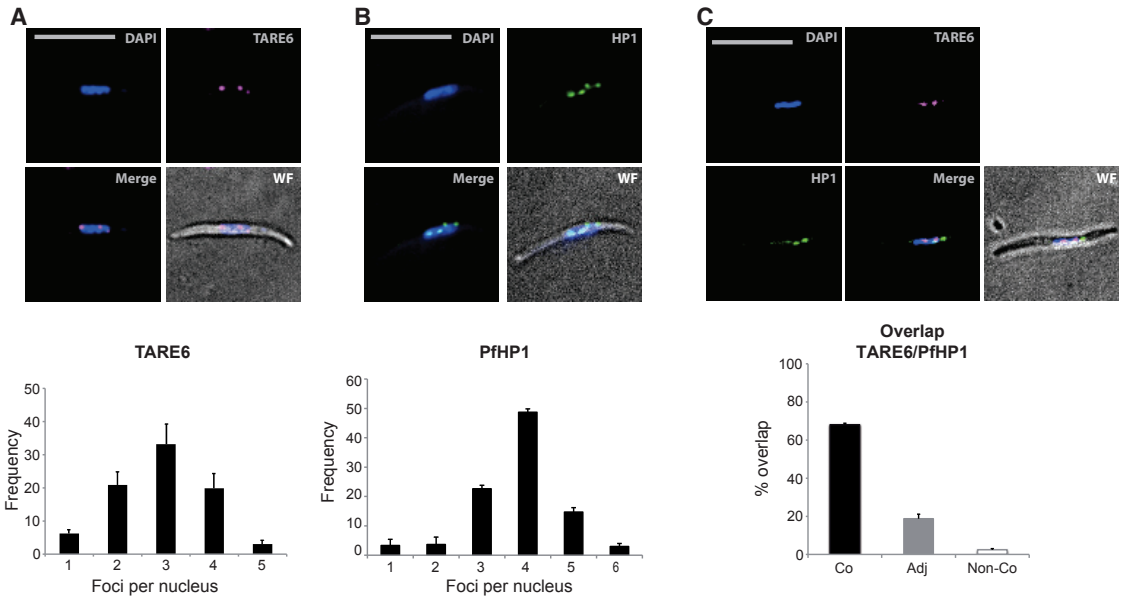

Figure 1. Chromosome Ends and Heterochromatin Islands Cluster at the Nuclear Periphery in *P. falciparum* Sporozoites

(A) DNA fluorescence *in situ* hybridization (FISH) of telomere distribution in sporozoites using a probe (magenta) against sub-telomeric repeat TARE6 (top) and corresponding quantification of the number of TARE6 foci per nucleus (bottom).

(B) Immunofluorescence of PfHP1 (green) in sporozoites using anti-PfHP1 antibodies (top) and corresponding quantification of the number of PfHP1 foci per nucleus (bottom).

For (A) and (B), error bars represent the 95% confidence intervals (±SEM) established for 50 sporozoites from three independent experiments.

(C) Combined DNA FISH of telomere distribution (using a TARE6 probe in magenta) and immunofluorescence of PfHP1 distribution (green) using anti-PfHP1 antibodies in sporozoites (top) and corresponding quantification of the percent overlap of TARE6 and PfHP1 foci per nucleus (bottom). Co, colocalized; Adj, adjacent; Non-Co, non-colocalized. Error bars represent SD from two independent experiments.

For (A)–(C), DNA was stained with DAPI (blue), and the wide-field (WF) image is merged with the fluorescent images. Scale bars, 5 μm.

and conditional depletion of PfHP1 disrupts transcriptional repression of *var* genes as well as the master regulator of sexual commitment, PfAP2-G (Brancucci et al., 2014). In addition, transcription of a single *var* gene is associated with antisense transcription of a long non-coding RNA (lncRNA) originating from its intron, a conserved feature shared by all members of the *var* family (Ralph et al., 2005; Jiang et al., 2013; Amit-Avraham et al., 2015). Thus, the parasite uses multiple layers of epigenetic regulation to ensure monoallelic expression of variant gene families, which creates phenotypic plasticity in genetically identical parasites during blood stage development (Lopez-Rubio et al., 2009; Rovira-Graells et al., 2012).

Although variegated gene expression appears to have evolved as a survival strategy to promote prolonged blood stage infections in humans, it is unknown whether heterochromatin-mediated control of variant gene families is important in other parasite stages, such as the sporozoite stage. Sporozoites have been successfully used to provide immune protection to human volunteers and are a key stage to target for malaria vaccine development (Richie et al., 2015).

To study the organization of heterochromatin in sporozoites, which are relatively low in abundance in the mosquito salivary glands, we developed a robust, low-cell-input chromatin immunoprecipitation followed by massively parallel sequencing (ChIP-seq) protocol. ChIP-seq of PfHP1 revealed a remarkable organization of heterochromatin in sporozoites that differs from that observed in asexual blood stage parasites. Furthermore, our epigenetic analysis predicted the expression of a specific PfEMP1 on the surface of sporozoites. Antibodies raised against this particular PfEMP1 efficiently blocked sporozoite infection of human hepatocytes in a strain-specific manner, demonstrating a previously unknown role of the *var* gene family in malaria parasite transmission.

RESULTS

Heterochromatin Islands Form Nuclear Clusters in Sporozoites

In *P. falciparum* blood stage parasites, the maintenance of heterochromatin islands is linked to the physical tethering of these genomic regions to the nuclear periphery, forming 4–7 perinuclear foci (Lopez-Rubio et al., 2009). PfHP1 is a major component of heterochromatin in perinuclear chromosome clusters. To determine whether a similar spatial chromosome arrangement exists in sporozoites, we performed DNA fluorescence in situ hybridization (FISH) using a probe corresponding to the conserved sub-telomeric repeat TARE6 (Telomere-Associated Repeat 6) (Figure 1A) and indirect immunofluorescene assays (IFAs) with antibodies against PfHP1 (Figure 1B). We observed an average of 2–4 TARE6-containing foci per nucleus, which localized to the nuclear periphery and overlapped with PfHP1-containing foci (Figure 1C). These data indicate

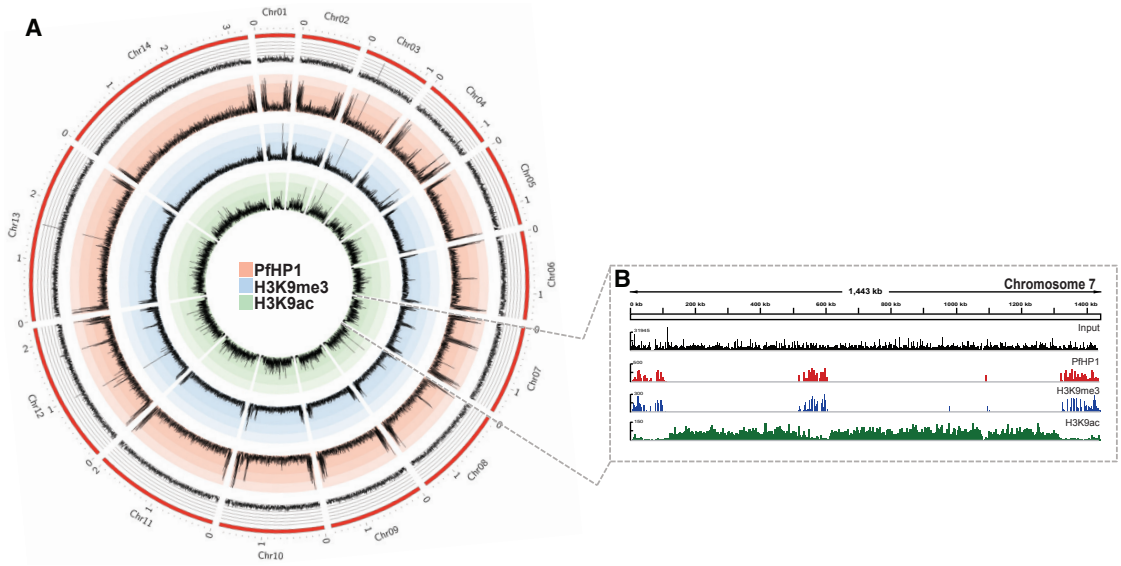

Figure 2. Genome-wide Distribution of Eu- and Heterochromatin in *P. falciparum* Sporozoites

(A) Circos plot of ChIP-seq data showing genome-wide enrichment of PfHP1 (red), H3K9me3 (blue), and H3K9ac (green) in sporozoites. Coverage plots are represented as average reads per million (RPM) over bins of 1,000 nt with a maximum y axis value of 400 for PfHP1, 500 for H3K9me3, and 400 for H3K9Ac. The 14 chromosomes are represented by the outer gray circle, with chromosome sizes given in megabases (Input, black). Statistical analysis of the biological replicates is presented in Table S1. MACS2-based peak calling analysis of PfHP1, H3K9me3, and H3K9ac enrichment in sporozoites is presented in Table S2.

(B) PfHP1, H3K9me3, and H3K9Ac enrichment across chromosome 7 in sporozoites, with genomic position indicated at the top in kilobases. Coverage plots are represented as average RPM over bins of 1,000 nt, with the maximum value of y axis indicated.

Data are representative of three or more independent experiments. See also Tables S1 and S2.

a conserved spatial organization of heterochromatin in the nucleus between asexual blood stage parasites and salivary gland sporozoites.

PfHP1 Genome-wide Distribution in *P. falciparum* Sporozoites

Previous studies have used ChIP to elucidate the role of histone post-translational modifications (PTMs), histone variants, and other chromatin factors in gene expression during the asexual stage of the human malaria parasite, *P. falciparum* (Lopez-Rubio et al., 2013). In asexual blood stages, PfHP1 and H3K9me3 regulate transcription of clonally variant virulence gene families such as *var* by establishing facultative heterochromatin at promoter regions and gene bodies (Lopez-Rubio et al., 2009; Flueck et al., 2009). These heterochromatic regions span approximately 100 kb, forming so-called heterochromatin islands at sub-telomeric regions and several internal chromosome clusters. Because the number of sporozoites that can be recovered from the infected mosquito salivary gland is low, we developed a robust low input ChIP-seq protocol, which allowed us to use approximately 600,000–800,000 sporozoites per immunoprecipitation (IP). We investigated the genome-wide distribution of heterochromatin by performing ChIP with highly specific antibodies against PfHP1 and the transcriptionally repressive histone H3 modification lysine 9 trimethylation (H3K9me3) (Tables S1 and S2). We observed an enrichment of PfHP1 and H3K9me3 in sub-telomeric regions of all 14 chromosomes, as well as in central chromosome regions of chromosomes 4, 6, 7, 8, and 12 (Figure 2A; Table S2). These regions contain variant gene families and show a similar heterochromatin enrichment in blood stage parasites (Lopez-Rubio et al., 2009). In contrast, ChIP-seq of the transcriptionally activating mark H3K9ac revealed its absence from these heterochromatic loci and enrichment within chromosome regions that primarily contain housekeeping genes (Figures 2A and 2B). Notably, ApiAP2-G, a member of the AP2 DNA-binding protein family that is involved in gametocyte formation, appears to be enriched in PfHP1 and H3K9me3 in sporozoites as it is in asexual blood stage parasites, suggesting a re-setting of the chromatin of this gene after gametogenesis is complete (Figure S1). We conclude that the heterochromatin organization is largely preserved in different life cycle stages.

Heterochromatin Spreads into Genes Coding for Exported Blood Stage Proteins in Sporozoites

When comparing the genome-wide PfHP1 pattern in sporozoites to that in asexual blood stage parasites (Figure 3A), we observed an overall similar organization of PfHP1 islands along all 14 chromosomes. We noted, however, a significant sporozoite-specific spreading of sub-telomeric heterochromatin from nearly all chromosome ends toward central chromosomal regions (Figures 3A and 3B). These extended heterochromatic regions of approximately 50 kb are highly enriched in genes encoding parasite proteins that are typically exported to the host erythrocyte during blood stage development, remodeling the erythrocyte to accommodate the parasite's needs (de Koning-Ward et al., 2016) (Figures 3B and S2). RNA sequencing in sporozoites showed that steady-state mRNA levels of these subtelomeric genes encoding

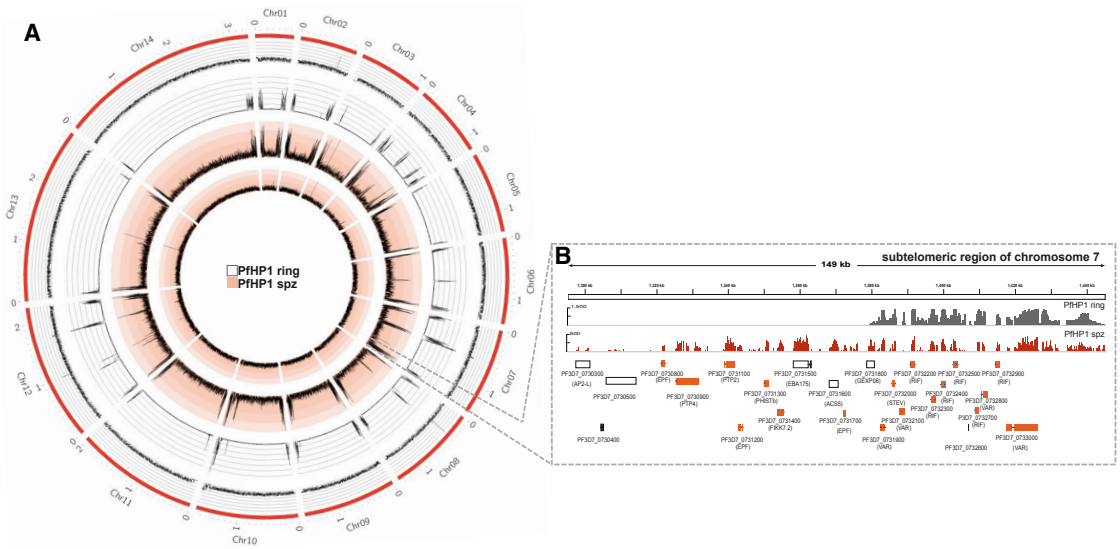

Figure 3. Heterochromatin Islands at Chromosome Ends Are Extended in *P. falciparum* Sporozoites Relative to Blood Stages

(A) Circos plot of ChIP-seq data compares genome-wide PfHP1 enrichment in sporozoites (spz; red lines) and asexual blood stage parasites (ring; gray lines). Coverage plots are represented as average RPM over bins of 1,000 nt with a y-axis maximum value of 400 for PfHP1 in sporozoites and 1,500 for PfHP1 in blood stages. The 14 chromosomes are represented by the outer gray circle, with chromosome sizes given in megabases. Statistical analysis of the biological replicates is presented in Table S1. MACS2-based peak calling analysis of PfHP1, H3K9me3, and H3K9ac enrichment in sporozoites is presented in Table S2.

(B) An enlarged view of a 149-kb sub-telomeric region of the right arm of chromosome 7 shows PfHP1 enrichment in the genomes of sporozoites (spz; red) and blood stage parasites (ring; black). Genes encoding exported proteins of iRBCs are highlighted in orange below the plot. Coverage plots are represented as average RPM over bins of 1 nt, with the maximum value indicated on the y axis.

Data are representative of three or more independent experiments. See also Tables S1 and S2.

blood-stage-exported proteins have an inverse correlation with H3K9me3/HP1 occupancy (Figure S3; Table S3), linking sporozoite heterochromatin extension to stage-specific gene silencing.

Heterochromatin Enrichment Predicts Expression of a *var* Gene in Sporozoites

In asexual blood stage parasites, a single PfEMP1 is expressed at any given time on the erythrocyte surface, and this expression correlates with low levels of PfHP1 and H3K9me3 within the promoter and gene body of the corresponding *var* gene. In contrast, the silent *var* genes are enriched for these heterochromatic marks (Lopez-Rubio et al., 2009). We performed MACS2-based peak enrichment analysis of four independent PfHP1 (Tables S2A and S4A) and three independent H3K9me3 (Table S2B) ChIP-seq sporozoite experiments. All *var* genes present in the NF54 *P. falciparum* strain were enriched for PfHP1 and H3K9me3 (Table S4A, "Peaks"). Intriguingly, one *var* gene (*PF3D7_0809100*) consistently showed the lowest enrichment of PfHP1 within its promoter and gene body (Figure 4A; Table S4A), suggesting that the corresponding PfEMP1 may be expressed in sporozoites. *PF3D7_0809100* (subsequently referred to as NF54*var*^{sporo}) is located in the central region of chromosome 8, adjacent to two other *var* genes and two members of a second clonally variant gene family *rif*, all of which retain higher levels of PfHP1 and H3K9me3 (Figure 4A). In general, other clonally variant gene families, including *rif*, *Pfmc2TM*, and *PfACS*, which are located proximal to sub-telomeric *var* genes on 13 of the 14 chromosomes, appear to maintain blood-stage-like heterochromatin patterns: only two of 180 *rif* genes, one of 13 *Pfmc2TM* genes, and five of 13 *PfACS* genes are depleted for PfHP1 and H3K9me3 (Table S5).

Given the major role of PfEMP1 in parasite virulence and immune evasion (Wahlgren et al., 2017), we focused on the expression of *var* genes in sporozoites. We investigated NF54*var*^{sporo} transcription by performing strand-specific RNA sequencing (RNA-seq) analysis of the sporozoite steady-state transcriptome (Figure S4; Table S3). As shown in Figure 4B (lower panel) and Figure 4C, we did not detect full-length mRNA transcripts for NF54*var*^{sporo} in the sporozoite (Tables S4B and S4C), but only bidirectional intronic promoter activity (Figure 4C, left panel) similar to that observed for silent *var* genes in the late-stage asexual blood stage parasites (Ralph et al., 2005; Epp et al., 2009). Despite identifying low-level, full-length mRNAs for two other *var* genes, *PF3D7_0711700* and *PF3D7_0412400* (Figure 4B, bottom panel; Figure S5; Tables S4B and S4C), these lack antisense noncoding RNAs (ncRNAs) to exon I that has been associated with *var* gene transcriptional activation and monoallelic expression in asexual blood stage parasites (Figure S5, left panel; and Table S4D) (Ralph et al., 2005; Jiang et al., 2013; Amit-Avraham et al., 2015). For this reason, we consider that *var* genes *PF3D7_0711700* and *PF3D7_0412400* may not be expressed in the sporozoite stage.

Since *var* mRNA transcription and PfEMP1 expression show limited overlap during asexual blood stage development, it is possible that NF54*var*^{sporo} is transcribed at the stage that precedes sporozoites: the oocysts in the mosquito midgut. Indeed, RNA-seq of oocysts (day 8 post-infection of the mosquito)

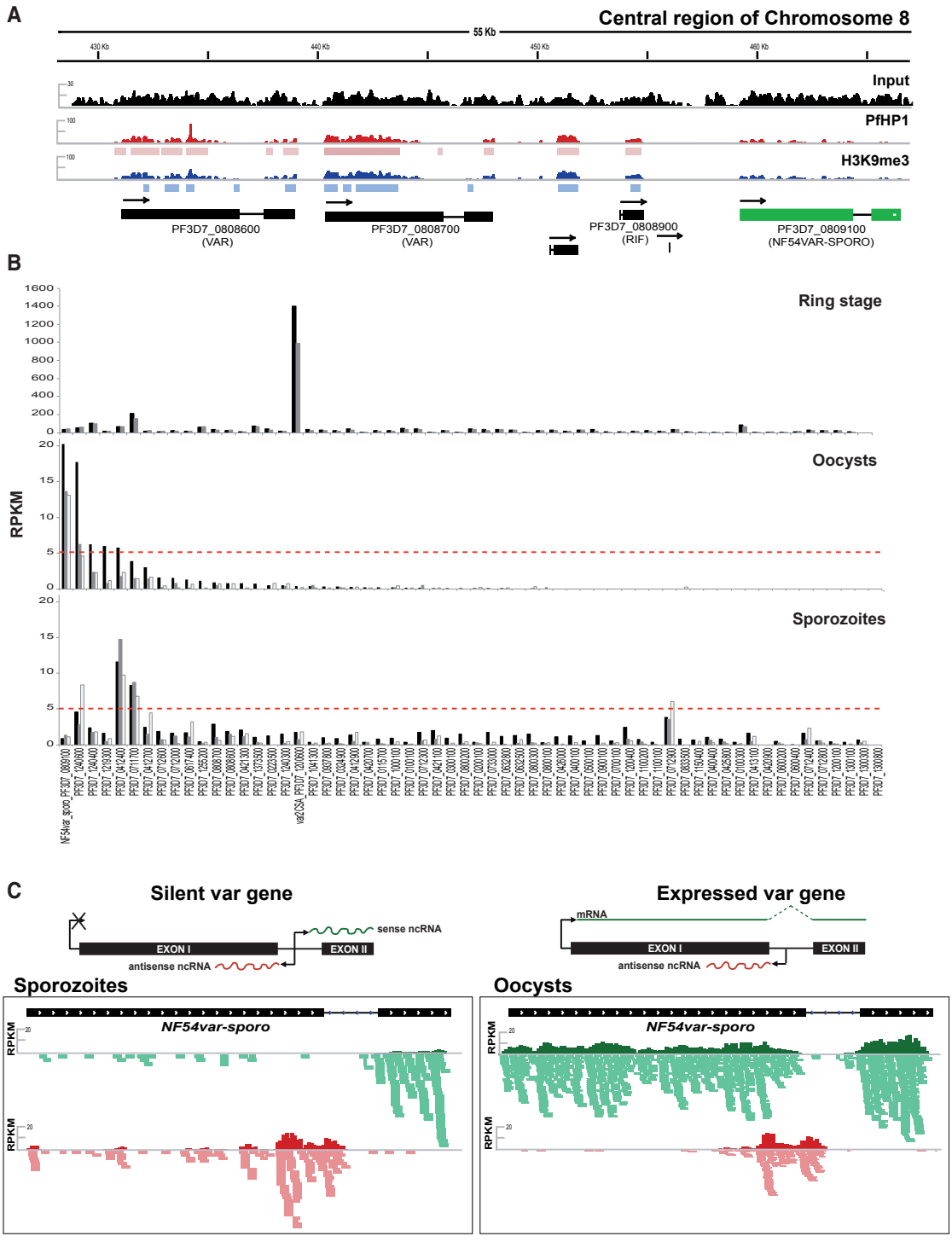

Figure 4. PfHP1 Occupancy Predicts Transcription of NF54*var*^{sporo} in Sporozoites

(A) ChIP sequencing data show enrichment of PfHP1 (red) and H3K9me3 (blue) over a 55-kb genomic region of chromosome 8 (chromosome coordinates are shown at top) in *P. falciparum* sporozoites. The coverage of the ChIP input DNA is indicated in black, and the MACS2-based peaks (Table S2) are indicated as rectangular boxes underneath the coverage plots. Coverage plots are represented as average RPM over bins of 1,000 nt with the maximum value indicated on the y axis. Data are representative of three or more independent experiments. The *var* gene *PF3D7_0809100*, or NF54*var*^{sporo}, shows low H3K9me3/PfHP1 enrichment and is highlighted in green.

(B) RNA-seq shows *var* gene transcription across different *P. falciparum* life-cycle stages: asexual-ring-stage parasites 12 hr post-invasion (two replicates at top), mosquito-derived oocysts (three replicates in the middle), and mosquito salivary gland sporozoites (three replicates at bottom). Transcripts corresponding to

(legend continued on next page)

revealed the presence of the full-length transcript of NF54*var*^{sporo}, which showed the highest RPKM (reads per kilobase of exon model per million reads) value of any *var* gene in three biological replicates (Figures 4B, middle panel, and 4C, right panel; Tables S4B and S4C), indicating that NF54_SpzPfEMP1 could be synthesized already in late mosquito stages. We observed another full-length *var* transcript, *PF3D7_1240600*; however, in the absence of intron-derived exon I antisense ncRNA, we speculate that this prohibits protein expression (Figure S5, right panel; Tables S4C and S4D). Alternatively, the observed oocyst *var* transcripts are expressed in individual parasites. Sporozoites expressing NF54*var*^{sporo} may have a selective advantage in the process of migration to the salivary gland, leading to, predominantly, sporozoites that express NF54_SpzPfEMP1.

In contrast, RNA-seq data from the parental ring asexual blood stage parasites detected almost no reads mapping to NF54*var*^{sporo} compared to the predominantly transcribed *var* gene, *PF3D7_1200600* (top panel of Figure 4B; Tables S4B and S4C), suggesting a reset of *var* gene transcription during the parasite transmission stage.

A Strain-Specific PfEMP1 Is Expressed on the Surface of Sporozoites

To determine whether the PfEMP1 protein encoded by NF54*var*^{sporo} is synthesized in sporozoites, we prepared NF54 sporozoite extracts and performed immunoblotting assays using either an antibody against the conserved intracellular C-terminal ATS (Acid Terminal Segment) domain that reacts with all PfEMP1 proteins (Nacer et al., 2015) or specific antibodies against the extracellular variable domain of NF54_SpzPfEMP1 (Figure 5A). Anti-NF54_SpzPfEMP1 antibodies and the anti-ATS reacted with a band corresponding to the predicted molecular weight of NF54_SpzPfEMP1 (241 kDa in Figures 5B and S6A). These sera detect smaller bands of approximately 70 to 75 KDa that may represent degraded forms of PfEMP1. Furthermore, IFAs of fixed NF54 sporozoites using mouse anti-NF54_SpzPfEMP1 and ATS antibodies showed a surface membrane-like staining pattern (Figure 5D). Almost all sporozoites (>98%) react with the anti-NF54_SpzPfEMP1 antibodies. We observed a similar IFA staining pattern in six independent NF54 sporozoite preparations, supporting the selective expression of a member of the *var* gene family. No surface staining was observed with antibodies against the extracellular domain of the PfEMP1 encoded by *var2CSA* (*Pf3D7_1200600*) or the CIDR (cysteine-rich interdomain region) domain of an unrelated central *var* gene (*Pf3D7_0412700*), both of which retain H3K9me3/PfHP1 enrichment in sporozoites (Figure S6B; data not shown).

Since NF54*var*^{sporo} is not conserved in other *P. falciparum* parasite strains (http://www.plasmodb.org) we performed IFA analysis on sporozoites of a genetically distinct strain, the Cambodian clone NF135 (Teirlinck et al., 2013). NF135 reacts with antibodies directed against the major surface antigen of sporozoites, Circumsporozoite protein (CSP) (Figure 5C). However, no cross-reactivity with anti-NF54_SpzPfEMP1 was observed. Expression of a PfEMP1 was confirmed by using anti-ATS (Figure 5D). These data suggest that an antigenically variant PfEMP1 antigen, possibly with a similar function as that of NF54_SpzPfEMP1, is expressed on the surface of NF135 *P. falciparum* sporozoites. Moreover, we performed blastp on the NF135 proteome (UniProt ID: UP000019114, based on the assembly deposited at GenBank [GEO: AOPS00000000], Broad Institute). No ortholog of NF54var^{sporo} was detectable in NF135, supporting the hypothesis that anti- NF54_SpzPfEMP1 antibodies do not crossreact with NF135 sporozoites.

The IFAs on live sporozoites, with intact cell membranes, and the anti-NF54_SpzPfEMP1 antibody, but not the anti-ATS antibody, stained the surface of sporozoites (Figure 5E). Trypsin treatment of live sporozoites (50 μg/mL) abolished antibody surface reactivity in immunofluorescence and by western blot, confirming that the CIDR domain of NF54_SpzPfEMP1 is extracellular in sporozoites (Figures 5B and 5E). Together, these results provide evidence of expression of a clonally variant and strain-specific PfEMP1 protein at the surface of sporozoites with a similar orientation to that seen at the membrane of iRBCs.

To study further the specificity of the anti-NF54_SpzPfEMP1, we incubated NF54 asexual blood stage parasites, with magnetic beads coated with immunoglobulin G (IgG) of anti-NF54_SpzPfEMP1. After three rounds of selection, we obtained parasites that react (>30%) with anti-NF54_SpzPfEMP1 (Figure S6C). qRT-PCR analysis on RNA prepared from ring stage parasites before and after panning showed an enrichment for NF54*var*^{sporo} transcripts of approximately 50-fold (Figure S6D). We demonstrate that the same PfEMP1 can be expressed in two distinct phases of the life cycle.

Antibodies against NF54_SpzPfEMP1 Block Sporozoite Infection of Hepatocytes

In intra-erythrocytic parasites, PfEMP1 proteins are exported across the parasite membrane and the parasitophorous vacuolar membrane to the surface of the erythrocyte, where they serve as adhesion molecules that can bind to a variety of endothelial receptors such as CD36, ICAM, etc., causing malaria pathogenesis by obstructing blood vessels in critical organs such as the brain (Wahlgren et al., 2017). Antibodies against the extracellular PfEMP1 region have been shown to block the rosetting phenotype and/or adhesion to various host endothelial receptors, such as CD36 or CSA.

Because NF54_SpzPfEMP1 is expressed on the surface of mature sporozoites, we evaluated its potential to interact with

exon I of each *var* gene (shown on the x axis) are indicated as RPKM (reads per kilobase of exon per one million mapped reads), indicated on the y axis. *var* gene transcription was only considered when above the red dotted line. See Table S4 for more details.
(C) Each *var* gene has two exons that flank a conserved intron. Shown in the top panel are schematics representing transcription of *var* mRNA and intronic ncRNAs from silent and active *var* genes. The bottom panel shows stranded RNA-seq data that demonstrate NF54*var*^{sporo} gene transcription in sporozoites (left) and oocysts (right). Coverage plots of steady-state RNA levels are indicated as RPKM (reads per kilobase of exon per one million mapped reads), with the mapped raw reads for sense (green) and antisense (red) transcription shown below the corresponding coverage plot.
See also Table S4.

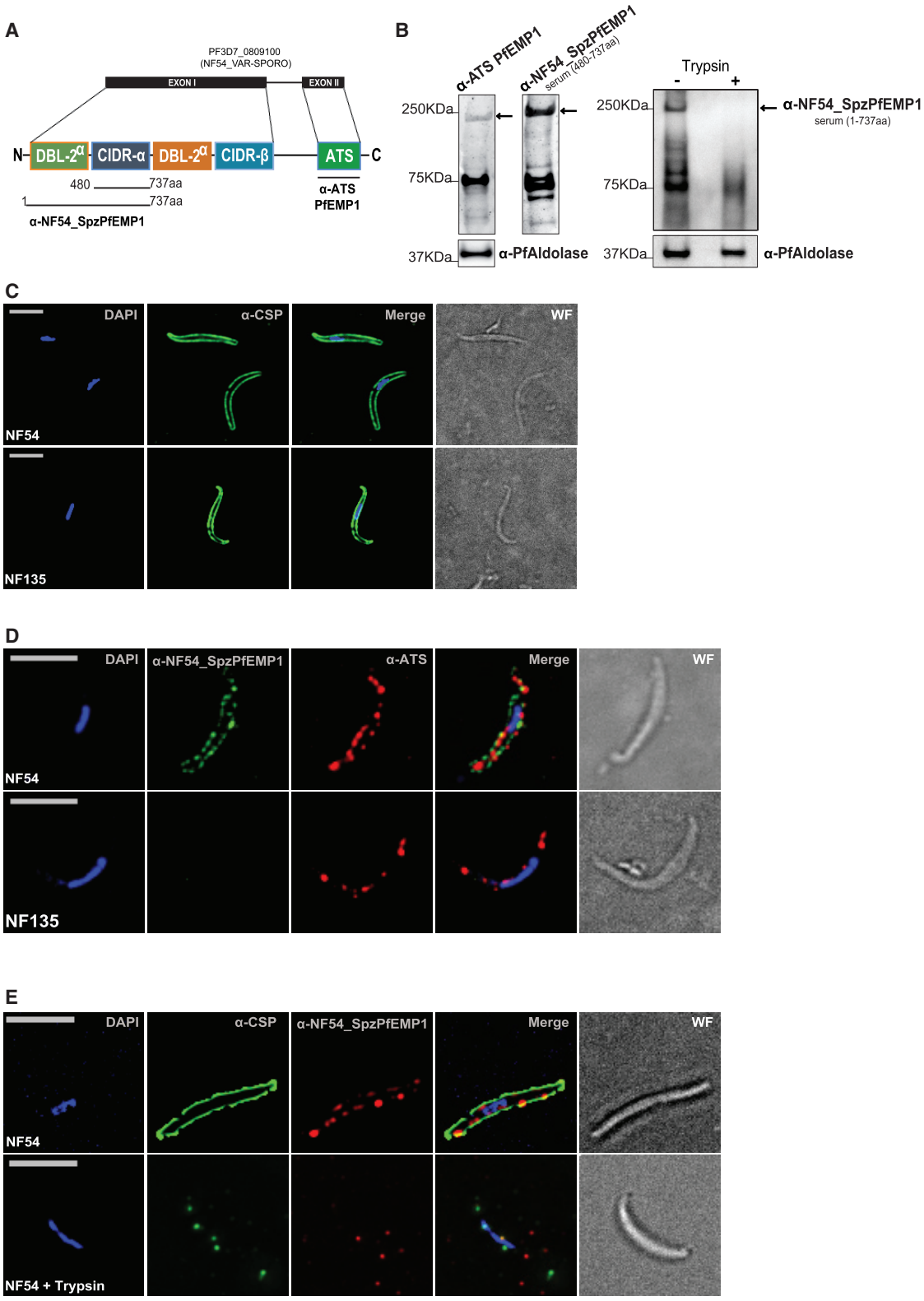

Figure 5. NF54_SpzPfEMP1 Protein Is Strain Specific and Exported to the Sporozoite Surface

(A) Schematic representation of the predicted domains of the PfEMP1 encoded by *PF3D7_0809100* and the corresponding antibodies against the semi-conserved ATS region and the polymorphic domains of the NF54_SpzPfEMP1.

(legend continued on next page)

hepatocytes, thus contributing to hepatocyte infection. We pre-incubated freshly isolated salivary gland sporozoites with either the anti-NF54_SpzPfEMP1 mouse antibody (both serum and the purified IgG) against the first 737 amino acids containing the DBL1 and CIDR1 domains (Figure 5A) or the corresponding pre-immune serum before adding the sporozoites to a primary human hepatocyte culture. After 3 days of infection, we observed that the anti-NF54_SpzPfEMP1 serum strongly reduced hepatocyte infection in a dilution-dependent manner, whereas the preimmune mouse serum showed only very low inhibition (Figure 6A). It is noteworthy that the purified anti-NF54_SpzPfEMP1 IgG (1.8 μg/mL) inhibits hepatocyte infection at a level similar to that of the anti-CSP IgG (20 μg/mL) (Figure 6A). Importantly, anti-NF54_SpzPfEMP1 did not block infection with clone NF135, which does not express NF54_SpzPfEMP1 (Figures 5D and 6A), whereas the anti-CSP antibody blocked both strains at levels >90% (Figure 6A).

Lastly, we assessed the immunogenicity of NF54_SpzPfEMP1 during natural infection. Serum of volunteers infected with NF54 sporozoites under chloroquine cover was obtained from a previous clinical trial that demonstrated that protective responses were mainly directed against *P. falciparum* pre-erythrocytic stages (Roestenberg et al., 2009) and was able to inhibit sporozoite invasion into hepatocytes (Peng et al., 2016). HEK293 cells expressing NF54_SpzPfEMP1, SEA-1 (*PF3D7_1021800*, positive control), or Etramp 14.2 (PF3D7_1476100, negative control) were incubated with serum and then subjected to fluorescence-assisted cell sorting. As shown in Figures 6B and 6C, the serum of one third of the infected volunteers contained significant antibody levels against NF54_SpzPfEMP1 (N-terminal CIDR region from amino acids 1–737), indicating that this PfEMP1 molecule is exposed on the surface of *P. falciparum* parasites before parasite blood stage infection develops.

DISCUSSION

Epigenetic regulation of *var* gene transcription and studies on the role of PfEMP1 in malaria pathogenesis have been focused on blood stage parasites (Guizetti and Scherf, 2013; Smith et al., 2013). Here, we present highly reproducible data from multiple NF54 sporozoite preparations that a specific member of the *var* multigene family (~60 members) is expressed in mosquito salivary gland parasites. Although we found that the overall nuclear organization is surprisingly conserved between asexual blood stage parasites and migratory sporozoite stages of *P. falciparum*, our developed ChIP-seq protocol for salivary gland stage sporozoites uncovered several features that provide insight into the biology of malaria transmission to humans. A striking feature is that subtelomeric heterochromatic region extends to genes that are exported into the host cell in asexual stages, adding a new parasite strategy to silence genes that are not used in free-living stages.

Our genome-wide analysis of PfHP1 and H3K9me3 enrichment predicted the expression of a member of the *var* gene family: *Pf3D7_0809100* or NF54*var*^{sporo}. Given that a bulk culture of the NF54 blood stage parasites express *var* genes that are distinct from NF54*var*^{sporo}, we propose that an epigenetic resetting of *var* genes occurs during mosquito stage development to select for expression of a specific PfEMP1 on the surface of sporozoites. We detect the NF54*var*^{sporo} transcript in late oocyst stage parasites, but this does not exclude the possibility that the resetting occurs at an earlier transmission stage. Regardless of when the epigenetic resetting occurs, our data suggest that, similar to asexual blood stage parasites, sporozoites may maintain monoallelic expression of *var* genes.

Our observation of epigenetic resetting of *var* genes is supported by transcriptional data obtained from blood stage parasites after passage through the mosquito. Studies with human volunteers have shown that *var* gene choice is altered upon mosquito transmission (Bachmann et al., 2016). A recent study reported the presence of a specific *var* gene transcript in sporozoites obtained from *P. falciparum*-infected patients from a malaria-endemic region in Africa; however, the authors did not report whether the corresponding PfEMP1 was produced (Gómez-Díaz et al., 2017). In light of these published data and our results, genetically different parasite strains may express antigenically variant PfEMP1 proteins in sporozoites.

Thus far, the biological role of the PfEMP1 surface adhesion molecule was believed to be restricted to immune evasion in the asexual blood stage. Our IFA data show that all salivary gland sporozoites express NF54_SpzPfEMP1 on their surface in a manner similar to that of iRBCs. It is currently unclear why a particular *var* gene member would be specifically targeted for mosquito stage expression. Structural analysis of NF54_SpzPfEMP1 does not reveal any specific features that would make it a particularly good candidate for expression at the sporozoite plasma membrane. One possibility is that the expression of a particular adhesive property may enhance sporozoite migration and hepatocyte infection. This hypothesis may limit the choice of expressed *var* gene for efficient transmission of parasites. The NF54*var*^{sporo} gene has not been studied before, and its adhesive features remain unknown.

Given that all asexual blood stage PfEMP1 proteins studied so far display adhesive properties (Smith, 2014), we hypothesized that NF54_SpzPfEMP1 plays a role in sporozoite interaction with various host tissues and infection of hepatocytes. Indeed, antibodies directed against the DBL and CIDR domains of NF54_SpzPfEMP1 resulted in very potent inhibition of hepatocyte

(B) Western blot analysis of sporozoite extracts using anti-ATS or anti-NF54_SpzPfEMP1 antibodies. Anti-PfAldolase antibodies served as a positive control for protein extraction. Molecular weights are shown at the left of the blot, and PfEMP1 is indicated with an arrow.
(C) Immunofluorescence analysis of fixed sporozoites of two different strains (NF54 at top and NF135 on bottom) using anti-CSP antibodies (green).
(D) Immunofluorescence analysis of fixed and permeabilized sporozoites of two different strains (NF54 at top and NF135 on bottom) using anti-NF54_SpzPfEMP1 (green) and anti-ATS (red) antibodies.
(E) Surface immunofluorescence of live sporozoites (top) and live sporozoites after trypsin treatment (bottom) using anti-CSP (green) and anti-NF54_SpzPfEMP1 (red) antibodies.
For (C)–(E), DNA was stained with DAPI (blue), and the wide-field (WF) image is shown at the right. Scale bars, 5 μm.

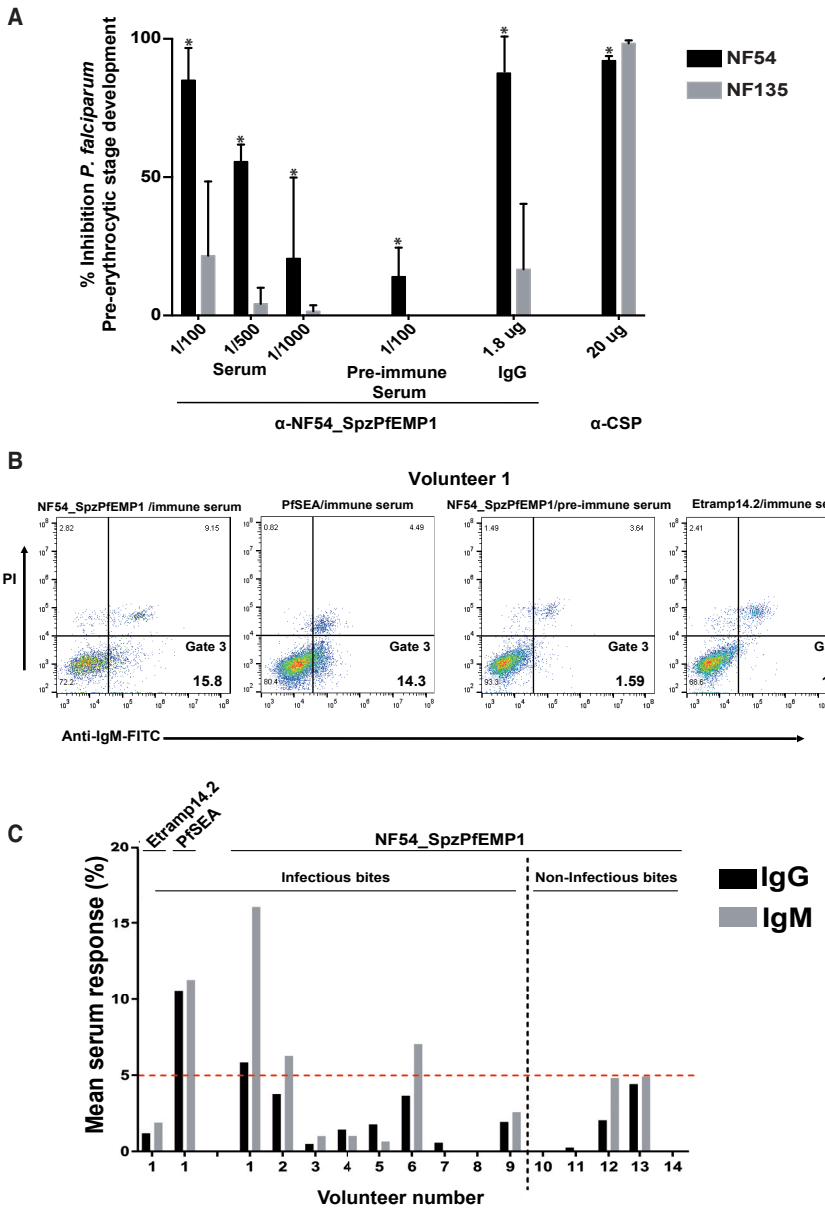

Figure 6. Antibodies against NF54_SpzPfEMP1 Inhibit Sporozoite Infection of Primary Human Hepatocytes

(A) NF54_SpzPfEMP1 antibody inhibition of hepatocyte infection of NF54 sporozoites expressing NF54_SpzPfEMP1 (black) and of NF135 sporozoites that did not express NF54_SpzPfEMP1 (gray). Data are presented as the percentage of inhibition over the untreated control after treatment with the following antibodies: anti-CSP, anti-NF54_SpzPfEMP1 immune serum, or the corresponding anti-NF54_SpzPfEMP1 pre-immune serum or purified IgG. Data represent the average of two independent biological experiments. *$p < 0.0205$, as measured using a two-way ANOVA. Error bars indicate SD.

(B and C) Detection of antibodies against NF54_SpzPfEMP1 in sera isolated from individuals immunized with infective bites and non-infective bites under chloroquine (CQ) prophylaxis. The sera were used to label HEK293 cells expressing NF54_SpzPfEMP1, schizont egress antigen (PfSEA; positive control), or Etramp14.2 (negative control), which were analyzed by flow cytometry. A second negative control used NF54_SpzPfEMP1 pre-immune sera to probe HEK293 cells expressing NF54_SpzPfEMP1.

(B) An anti-IgM (immunoglobulin M)-FITC (fluorescein isothiocyanate) signal (x axis) indicates specific binding, and a propidium iodide (PI) signal (y axis) indicates dead cells. Gate 3 consists of cells positive for IgM staining for either NF54_SpzPfEMP1, PfSEA, or Etramp.

(C) Quantification of the serum IgG (black) or IgM (gray) response from all individuals in the chloroquine sera set as measured by fluorescence-activated cell sorting (FACS). Individual volunteers are shown on the x axis, and the mean of three technical replicates of serum response is shown on the y axis. Serum response was considered significant when above the red dotted cutoff line, using the Mann-Whitney U test. Serum response was determined as the ratio of the population of cells with bound sera antibodies to the population of transfected cells (transfection efficiency). It is expressed as a percentage illustrated as follows: serum response = (cell population with bound sera antibodies/cell population that is transfected) × 100%.

infection. In the future, genetically modified parasites that either lack the NF54*var*^{sporo} *var* gene or express genetically modified extracellular PfEMP1 domains may help to elucidate the function of NF54_SpzPfEMP1 during the various mosquito stages and, perhaps, even hepatocyte infection.

Our work is highly relevant to vaccine development based on live-attenuated sporozoites. Sterile protection in human volunteers has been reported after challenge with homologous, laboratory-adapted *P. falciparum* sporozoites (Kublin et al., 2017). Given our discovery that a clonally variant antigen on the surface of sporozoites is expressed in a strain-specific manner, one may speculate that natural protective immune responses target variant sporozoite surface antigens such as PfEMP1. This could impact the efficacy of a sporozoite vaccine in patients from distinct geographic regions, as has been recently reported (Schats et al., 2015). It is noteworthy that PfEMP1 does not exist in rodent models that are often used for sporozoite vaccine evaluation. Thus, prediction of vaccine efficacy in these models does not take into account the expression of *P. falciparum* species-specific variant molecules.

In conclusion, this study provides evidence for the sporozoite-specific repurposing of the PfEMP1 surface antigen family, the biological function of which was thought to be restricted to immune evasion (antigenic variation) during chronic blood stage infection in the human host. Our discovery of a strain-specific surface antigen may provide a molecular explanation for the reduced protection of human volunteers after challenge with heterologous *P. falciparum* sporozoites. As our data demonstrate

an unprecedented role of PfEMP1 proteins in transmission stages and provide insight into the biology of sporozoites during infection of hepatocytes, this work is highly relevant for vaccine design based on sporozoites.

EXPERIMENTAL PROCEDURES

Human Plasma Samples

Samples were obtained from a previous clinical trial carried out at the Radboud University Nijmegen Medical Center (Nijmegen, the Netherlands), in accordance with principles of good clinical practice and with prior approval from the Central Committee for Research Involving Human Subjects of the Netherlands (NCT00442377). Study subjects (n = 14) were exposed to either infective (n = 9) or non-infective (n = 5) mosquito bites with concurrent chloroquine prophylaxis (Roestenberg et al., 2009).

Isolation and Purification of *P. falciparum* Sporozoites and Oocysts

Adult *Anopheles stephensi* females were infected with either *P. falciparum* strain NF54 (originating from West Africa) or strain NF135, clone C10 (originating from Cambodia) as previously described (Ponnudurai et al., 1989; Teirlinck et al., 2013). For each biological replicate, sporozoites were obtained by aseptically dissecting salivary glands of 200–400 infected mosquitoes 14–21 days after an infective blood meal. Pooled salivary glands were homogenized, filtered with a 40-μm cell strainer, and purified on a 17% Accudenz gradient as previously described (Kennedy et al., 2012). For each biological replicate, oocysts were isolated by dissection of the midguts of 50 infected mosquitoes, with an average of 45 oocysts per mosquito, 8 days post-infection. Biological replicates came from independent rounds of mosquito infection.

ChIP and Next-Generation Sequencing

ChIP was performed as previously described (Lopez-Rubio et al., 2009), using 5×10^6 *P. falciparum* sporozoites (strain NF54) or 10^9 asexual ring stage parasites (strain 3D7, clone G7). For each ChIP experiment, 0.5 μg anti-H3K9me3 (Millipore #07-442), anti-H3K9ac (Millipore #07-352), or anti-PfHP1 (Chen et al., 2016) rabbit polyclonal antibodies was used. To generate Illumina-compatible sequencing libraries, the immunoprecipitated DNA was processed using the MicroPlex Library Preparation Kit (Diagenode) according to the manufacturer's instructions. As a control, DNA corresponding to the ChIP input or DNA immunoprecipitated using rabbit IgG (Diagenode, #C15410206) was processed. Pooled, multiplexed libraries were subjected to 150-bp single-end sequencing on an Illumina NextSeq 500. The resulting data were demultiplexed using bcl2fastq2 (Illumina) to obtain fastq files for downstream analysis. A minimum of three biological replicates was analyzed for each antibody and each parasite stage (Table S6).

ChIP-Seq Data Analysis

Quality control of fastq files was performed using the FastQC software (http://www.bioinformatics.babraham.ac.uk/projects/fastqc/). Sequencing reads were mapped to the *P. falciparum* genome (Gardner et al., 2002; PlasmoDB, v.3) with the Burrows-Wheeler Alignment tool (BWA-MEM algorithm) using default parameters (Li and Durbin, 2009). Uniquely mapped reads were filtered for duplicates and an alignment quality Phred score (Q) ≥ 20 using samtools (Li et al., 2009). The ChIP-seq data were normalized over input. Peak-calling analysis was performed with the MACS2 software (Zhang et al., 2008) with default settings and a false discovery rate cutoff of 5%, using Benjamini and Hochberg's correction method. For genome-wide representation of PfHP1, H3K9ac, and H3K9me3 distribution, the coverage of each chromatin mark was calculated as average reads per million over bins of 1,000 nt using bamCoverage from the package deepTools2 (Ramírez et al., 2016), unless otherwise specified. Correlation of the different biological replicates was determined using MACS2, bedtools (Quinlan and Hall, 2010), and deepTools2. Circular and linear coverage plots were generated using Circos (Krzywinski et al., 2009) and Integrated Genomics Viewer (Thorvaldsdóttir et al., 2013), respectively.

RNA-Seq Library Preparation and Data Analysis

For RNA-seq library preparation, total RNA from sporozoites, oocysts, or asexual ring stage parasites was extracted using the miRNeasy Mini Kit (QIAGEN) according to the manufacturer's instructions, including on-column DNase digestion. Total RNA was poly(A)-enriched using the Dynabeads mRNA Purification Kit (Life Technologies) and subjected to strand-specific RNA-seq library preparation using the TruSeq Stranded mRNA Library Prep Kit (Illumina). The libraries were multiplexed and subjected to 150-bp single-end sequencing on an Illumina NextSeq 500. The resulting data were demultiplexed using bcl2fastq2 (Illumina) to obtain fastq files for downstream analysis. A minimum of two biological replicates was analyzed for each parasite stage (Table S6).

As described earlier, quality control of fastq files was performed using FastQC software and sequencing reads mapped to the *P. falciparum* genome (Gardner et al., 2002, PlasmoDB, v.3) with the Burrows-Wheeler Alignment tool (BWA-MEM algorithm) using default parameters. Gene counts (i.e., the number of aligned reads mapping to different genomic loci) were calculated using bedtools (Quinlan and Hall, 2010). Differential gene expression analysis was performed using the R package edgeR (Robinson et al., 2010).

Multidimensional scaling (MDS) plots were also made in edgeR using "plotMDS," where distances between pairs of RNA samples correspond to the leading $\log_2$ fold changes (i.e., average [root-mean-square] of the largest absolute $\log_2$ fold changes) (Robinson et al., 2010). To generate coverage plots, the gene counts normalized for gene length and sequencing depth by calculating RPKM values in the R:limma package (Ritchie et al., 2015). Coverage plots were visualized using the Integrated Genomics Viewer (Robinson et al., 2011; Thorvaldsdóttir et al., 2013).

DNA Fluorescence *In Situ* Hybridization and Immunofluorescence Imaging

Sporozoites were fixed in suspension with 4% paraformaldehyde (PFA) in PBS (pH 7.4) overnight at 4°C. After three PBS washes, parasites were resuspended in PBS, and deposited on poly-L-lysine-coated #1.5 coverslips (Marienfeld Superior). Parasites were permeabilized with 0.1% Triton X-100 for 15 min and subjected to DNA FISH labeling with the TARE6 probe as described previously for blood stage parasites (Mancio-Silva et al., 2008). Immunofluorescent labeling using rabbit anti-PfHP1 antibodies was performed as previously described (Chen et al., 2016). For combined DNA FISH and immunofluorescence, sporozoites were first labeled with rabbit anti-PfHP1 antibodies (diluted 1:2,000 in 3% BSA [Sigma] in PBS) and then with anti-rabbit Alexa Fluor 488 secondary antibodies (Life Technologies). After an additional fixation step with 4% PFA, DNA FISH was performed using a biotinylated locked nucleic acid (LNA) probe (Exiqon) targeting all TARE6 telomeric repeats (5′-Biotin-+AC+T+AACA+TA+GG+T+CT+T+A-Biotin-3′), which was then detected with streptavidin-conjugated Alexa Fluor 568 secondary antibodies (Life Technologies).

NF54_SpzPfEMP1 Protein Expression and Antibody Generation

The DNA sequence encoding the CIDR-alpha of *PF3D7_0809100* was cloned into the *Baculovirus* transfer vector pAcGP67-A (BD Biosciences). Recombinant CIDR product was expressed by infection of insect High Five cells with recombinant *Baculovirus*. Antibodies to *Baculo*-expressed CIDR were raised in Wistar rats by subcutaneous injection as previously described (Bengtsson et al., 2013). All experimental animal procedures were approved by The Danish Animal Procedures Committee ("Dyreforsøgstilsynet") as described in permit no. 2008/561-1498 and according to the guidelines described in Danish acts LBK 1306 (23/11/2007) and BEK 1273 (12/12/2005). For the mouse, anti-NF54_SpzPfEMP1 antibody production, a codon-optimized synthetic gene encoding amino acids 1–737 of *PF3D7_0809100* was synthesized by GenScript Biotech and cloned into the pET28 vector. Recombinant protein was produced using SHuffle T7 Express bacteria (New England BioLabs), and soluble protein was purified using Ni-NTA His Bind Superflow Resin (Novagen) according to manufacturer's instructions. Purified protein (10 μg of >90% purity) was used to immunize C57BL/6 mice. Animal care and experiments involving mice were conducted at the Institute Pasteur with the approval of the Direction Départementale des Services Vétérinaires of Paris, France (permit no. 75-066, issued on September 14, 2009) and

performed in compliance with institutional guidelines and European regulations (http://ec.europa.eu/environment/chemicals/lab_animals/index_en.htm). A statement of compliance with the French government's ethical and animal experiment regulations was issued by the Ministère de l'Enseignement Supérieur et de la Recherche under the number 00218.01.

Western Blot Analysis

5×10^6 *P. falciparum* NF54 sporozoites were resuspended in 100 μL 2× NuPAGE sample buffer supplemented with reducing agent (Thermo Fisher Scientific) and incubated at 95°C for 5 min, after which DNA was sheared. The resulting sporozoite protein extract was resolved on a 3%–8% Tris-Acetate SDS-polyacrylamide gel (NuPAGE) using MOPS SDS Running Buffer (Thermo Fisher Scientific) and transferred to a PVDF membrane. The membrane was blocked for 1 hr with 5% milk in TBST (50 mM Tris, 150 mM NaCl, 0.1% Tween 20). PfEMP1 proteins were detected using guinea pig anti-ATS antibodies (Nacer et al., 2015) or anti-NF54_SpzPfEMP1 antibodies. PfAldolase was detected with anti-PfAldolase-HRP (horseradish peroxidase) antibodies (Abcam, ab38905). Primary antibodies were detected by goat anti-guinea pig-HRP (Abcam, ab6908), anti-rat-HRP, or anti-mouse-HRP (GE Healthcare Life Sciences, NA935V and NA931V, respectively) secondary antibodies. HRP signal was developed with SuperSignal West Pico chemiluminescent substrate (Thermo Fisher Scientific, #34080) and imaged with a ChemiDoc XRS+ System (Bio-Rad). Images were analyzed using the Fiji image processing package (http://fiji.sc).

Immunofluorescence Assay

NF54 or NF135 sporozoites were placed on poly-L-lysine-coated coverslips for 10 min at room temperature (RT) under one of three conditions: live or fixed in 4% PFA and permeabilized with 0.01% Triton X-100. The cells were blocked with 4% BSA in PBS for 30 min at RT and then incubated with primary antibody for 1 hr at RT; dilutions were 1:1,000 for anti-ATS, 1:1,000 for anti-NF54_SpzPfEMP1, 1:200 for anti-var2CSA (Avril et al., 2011), and 1:15,000 for anti-CSP (Okitsu et al., 2007) antibodies in 3% BSA in PBS. After three washes with PBS, primary antibodies were detected with Alexa Fluor 488- or 568-conjugated secondary antibodies (Life Technologies) diluted 1:1,000 in 3% BSA in PBS. After three final washes in PBS, cells were mounted in Vectashield containing DAPI for nuclear staining. Images were captured using a Deltavision Elite imaging system (GE Healthcare). Image processing of at least two independent replicates was performed using the Fiji package (http://fiji.sc). For trypsinization prior to imaging, 10^6 living sporozoites were treated with trypsin (GIBCO, 50 mg/mL in 200 μL Leibovitz's L-15 medium) for 40 min at RT. Sporozoites were then washed three times with Leibovitz's L-15 medium containing serum and processed as described earlier, with all incubations on ice.

Liver Stage Development Inhibition Assay

Primary human hepatocyte cultures were prepared from two different batches of human hepatocytes following the manufacturer's instructions. Briefly, cryopreserved human hepatocytes (Biopredic International) were thawed and resuspended in seeding medium according to the manufacturer's instructions. Cells were seeded in 96-well plates previously coated with rat tail collagen I (BD Biosciences), and after cell attachment, a Matrigel (BD Biosciences) overlay was added. 24 hr after plating, medium was replaced with culture medium (William's medium E, Life Technologies) supplemented with 10% fetal calf serum (FCS; Perbio), 5×10^{-5} M hydrocortisone hemisuccinate (Upjohn Laboratories SERB, Paris, France), 5 μg/mL human insulin (Sigma), 2 mM L-glutamine, 100 U/mL penicillin, and 100 μg/mL streptomycin (Life Technologies). The heat-inactivated mouse sera containing anti-NF54_SpzPfEMP1 antibodies (diluted 1:100, 1:500, or 1:1000), the correspondent pre-immune sera (diluted 1:100), or the purified anti-NF54_SpzPfEMP1 IgG (diluted 1:100) were added to 50 μL medium containing 3×10^4 *P. falciparum* NF54 or NF135 sporozoites. The Matrigel overlay was removed from the infected human hepatocyte culture before addition of the mixture of antibodies and sporozoites. Plates were centrifuged at 2,000 rpm for 10 min at RT to facilitate parasite settling onto the cells. Medium was changed 3 hr post-infection, and Matrigel was added to the infected culture; medium was replaced 48 hr post-addition of sporozoites. Cultures were stopped at day 3 post-infection by fixing with cold methanol. Parasite numbers within hepatocytes were assessed via immunofluorescence using anti-PfHSP70 antibodies as previously described (Rénia et al., 1990). Quantification was performed by microscopy or by using the ArrayScan XTI imaging system (Thermo Fisher Scientific).

Determination of Serum Response against NF54_SpzPfEMP1

Sera isolated from individuals from a previous clinical trial (Roestenberg et al., 2009) were used to probe HEK293 cells transfected for cell-surface expression of *P. falciparum* proteins. For NF54_SpzPfEMP1, a DNA construct encoding amino acids 1–737 was used for transfection. These HEK293 cells were analyzed by flow cytometry, as previously described (Peng et al., 2016). Serum response was defined as the percentage of transfected cells that show bound serum antibodies (Peng et al., 2016). For sera with positive serum response (>5%), the serum response against *var*-transfected cells was compared with the serum response against Etramp14.2-transfected cells (negative control), using the Mann Whitney U test, and was found to be significantly higher.

Parasite Panning on Antibody-Coated Magnetic Beads

Sterile Dynabeads Protein G (Life Technologies 10003D) were incubated with 20 μg filtered anti-NF54_SpzPfEMP1 IgG for 10 min at RT under agitation. The Dynabeads were blocked with 1% BSA for 20 min. iRBCs containing trophozoites and schizonts were isolated by plasmagel enrichment and resuspended in 400 μL PBS at a concentration of 5×10^7 iRBCs per milliliter. The iRBCs and the beads were mixed by gently pipetting and allowed to bind for 1 hr with gentle agitation at 37°C. After incubation, the beads were washed 8 times with 800 μL sterile PBS to eliminate all unbound cells. Bound cells were resuspended with culture medium and fresh red blood cells. In total, three antibody pannings were performed. The enrichment was assessed after each panning by IFA using anti-NF54_SpzPfEMP1.

DATA AND SOFTWARE AVAILABILITY

The accession number for the ChIP-seq and RNA-seq fastq files generated in this study is NCBI: PRJNA344838. To understand the files, please refer to Table S6.

SUPPLEMENTAL INFORMATION

Supplemental Information includes six figures and six tables and can be found with this article online at https://doi.org/10.1016/j.celrep.2018.02.075.

ACKNOWLEDGMENTS

We thank Benoit Gamain for providing anti-var2CSA antibodies. This work was supported by a European Research Council advanced grant (PlasmoSilencing 670301) to A.S., by an ANR grant HypEpiC (ANR-14-CE16-0013) to D. Mazier and A.S., and by the French Parasitology consortium ParaFrap (ANR-11-LABX0024) to A.S. and D. Mazier. G.Z. and S.D. were supported by a ParaFrap PhD fellowship, S.S.V. was supported by a Carnot-Pasteur-Maladies Infectieuse fellowship, and J.B. was supported by an EMBO fellowship (ALTF 180-2015).

AUTHOR CONTRIBUTIONS

Conceptualization, G.Z., S.S.V., D. Mazier, and A.S.; Methodology, G.Z. and S.S.V.; Investigation, G.Z., S.S.V., S.D., S.B., J.G., J.-F.F., M.B., V.S., O. Silvie, R.S., L.R., Y.S.G., and J.M.B. Writing – Original Draft, G.Z., S.S.V., and A.S.; Writing – Review & Editing, G.Z. and A.S.; Resources, D. Mattei, P.C., S.M., C.C.H., O. Scatton, and A.T.R.J.; Funding Acquisition, A.S.

DECLARATION OF INTERESTS

The authors declare no competing interests.

Received: August 9, 2017
Revised: January 22, 2018
Accepted: February 17, 2018
Published: March 13, 2018

REFERENCES

Amit-Avraham, I., Pozner, G., Eshar, S., Fastman, Y., Kolevzon, N., Yavin, E., and Dzikowski, R. (2015). Antisense long noncoding RNAs regulate var gene activation in the malaria parasite *Plasmodium falciparum*. Proc. Natl. Acad. Sci. USA *112*, E982–E991.

Avril, M., Hathaway, M.J., Srivastava, A., Dechavanne, S., Hommel, M., Beeson, J.G., Smith, J.D., and Gamain, B. (2011). Antibodies to a full-length VAR2CSA immunogen are broadly strain-transcendent but do not cross-inhibit different placental-type parasite isolates. PLoS ONE *6*, e16622.

Bachmann, A., Petter, M., Krumkamp, R., Esen, M., Held, J., Scholz, J.A., Li, T., Sim, B.K., Hoffman, S.L., Kremsner, P.G., et al. (2016). Mosquito passage dramatically changes *var* gene expression in controlled human *Plasmodium falciparum* infections. PLoS Pathog. *12*, e1005538.

Bengtsson, A., Joergensen, L., Rask, T.S., Olsen, R.W., Andersen, M.A., Turner, L., Theander, T.G., Hviid, L., Higgins, M.K., Craig, A., et al. (2013). A novel domain cassette identifies *Plasmodium falciparum* PfEMP1 proteins binding ICAM-1 and is a target of cross-reactive, adhesion-inhibitory antibodies. J. Immunol. *190*, 240–249.

Brancucci, N.M.B., Bertschi, N.L., Zhu, L., Niederwieser, I., Chin, W.H., Wampfler, R., Freymond, C., Rottmann, M., Felger, I., Bozdech, Z., and Voss, T.S. (2014). Heterochromatin protein 1 secures survival and transmission of malaria parasites. Cell Host Microbe *16*, 165–176.

Chen, P.B., Ding, S., Zanghì, G., Soulard, V., DiMaggio, P.A., Fuchter, M.J., Mecheri, S., Mazier, D., Scherf, A., and Malmquist, N.A. (2016). *Plasmodium falciparum* PfSET7: enzymatic characterization and cellular localization of a novel protein methyltransferase in sporozoite, liver and erythrocytic stage parasites. Sci. Rep. *6*, 21802.

de Koning-Ward, T.F., Dixon, M.W., Tilley, L., and Gilson, P.R. (2016). *Plasmodium* species: master renovators of their host cells. Nat. Rev. Microbiol. *14*, 494–507.

Epp, C., Li, F., Howitt, C.A., Chookajorn, T., and Deitsch, K.W. (2009). Chromatin associated sense and antisense noncoding RNAs are transcribed from the *var* gene family of virulence genes of the malaria parasite *Plasmodium falciparum*. RNA *15*, 116–127.

Flueck, C., Bartfai, R., Volz, J., Niederwieser, I., Salcedo-Amaya, A.M., Alako, B.T., Ehlgen, F., Ralph, S.A., Cowman, A.F., Bozdech, Z., et al. (2009). *Plasmodium falciparum* heterochromatin protein 1 marks genomic loci linked to phenotypic variation of exported virulence factors. PLoS Pathog. *5*, e1000569.

Gardner, M.J., Hall, N., Fung, E., White, O., Berriman, M., Hyman, R.W., Carlton, J.M., Pain, A., Nelson, K.E., Bowman, S., et al. (2002). Genome sequence of the human malaria parasite *Plasmodium falciparum*. Nature *419*, 498–511.

Gómez-Díaz, E., Yerbanga, R.S., Lefèvre, T., Cohuet, A., Rowley, M.J., Ouedraogo, J.B., and Corces, V.G. (2017). Epigenetic regulation of Plasmodium falciparum clonally variant gene expression during development in Anopheles gambiae. Sci. Rep. *7*, 40655.

Guizetti, J., and Scherf, A. (2013). Silence, activate, poise and switch! Mechanisms of antigenic variation in Plasmodium falciparum. Cell. Microbiol. *15*, 718–726.

Jiang, L., Mu, J., Zhang, Q., Ni, T., Srinivasan, P., Rayavara, K., Yang, W., Turner, L., Lavstsen, T., Theander, T.G., et al. (2013). PfSETvs methylation of histone H3K36 represses virulence genes in *Plasmodium falciparum*. Nature *499*, 223–227.

Kennedy, M., Fishbaugher, M.E., Vaughan, A.M., Patrapuvich, R., Boonhok, R., Yimamnuaychok, N., Rezakhani, N., Metzger, P., Ponpuak, M., Sattabongkot, J., et al. (2012). A rapid and scalable density gradient purification method for *Plasmodium* sporozoites. Malar. J. *11*, 421.

Krzywinski, M., Schein, J., Birol, I., Connors, J., Gascoyne, R., Horsman, D., Jones, S.J., and Marra, M.A. (2009). Circos: an information aesthetic for comparative genomics. Genome Res. *19*, 1639–1645.

Kublin, J.G., Mikolajczak, S.A., Sack, B.K., Fishbaugher, M.E., Seilie, A., Shelton, L., VonGoedert, T., Firat, M., Magee, S., Fritzen, E., et al. (2017). Complete attenuation of genetically engineered Plasmodium falciparum sporozoites in human subjects. Sci. Transl. Med. *9*, eaad9099.

Li, H., and Durbin, R. (2009). Fast and accurate short read alignment with Burrows-Wheeler transform. Bioinformatics *25*, 1754–1760.

Li, H., Handsaker, B., Wysoker, A., Fennell, T., Ruan, J., Homer, N., Marth, G., Abecasis, G., and Durbin, R.; 1000 Genome Project Data Processing Subgroup (2009). The Sequence Alignment/Map format and SAMtools. Bioinformatics *25*, 2078–2079.

Lopez-Rubio, J.J., Mancio-Silva, L., and Scherf, A. (2009). Genome-wide analysis of heterochromatin associates clonally variant gene regulation with perinuclear repressive centers in malaria parasites. Cell Host Microbe *5*, 179–190.

Lopez-Rubio, J.J., Siegel, T.N., and Scherf, A. (2013). Genome-wide chromatin immunoprecipitation-sequencing in Plasmodium. Methods Mol. Biol. *923*, 321–333.

Mancio-Silva, L., Rojas-Meza, A.P., Vargas, M., Scherf, A., and Hernandez-Rivas, R. (2008). Differential association of Orc1 and Sir2 proteins to telomeric domains in *Plasmodium falciparum*. J. Cell Sci. *121*, 2046–2053.

Nacer, A., Claes, A., Roberts, A., Scheidig-Benatar, C., Sakamoto, H., Ghorbal, M., Lopez-Rubio, J.J., and Mattei, D. (2015). Discovery of a novel and conserved *Plasmodium falciparum* exported protein that is important for adhesion of PfEMP1 at the surface of infected erythrocytes. Cell. Microbiol. *17*, 1205–1216.

Okitsu, S.L., Kienzl, U., Moehle, K., Silvie, O., Peduzzi, E., Mueller, M.S., Sauerwein, R.W., Matile, H., Zurbriggen, R., Mazier, D., et al. (2007). Structure-activity-based design of a synthetic malaria peptide eliciting sporozoite inhibitory antibodies in a virosomal formulation. Chem. Biol. *14*, 577–587.

Peng, K., Goh, Y.S., Siau, A., Franetich, J.F., Chia, W.N., Ong, A.S., Malleret, B., Wu, Y.Y., Snounou, G., Hermsen, C.C., et al. (2016). Breadth of humoral response and antigenic targets of sporozoite-inhibitory antibodies associated with sterile protection induced by controlled human malaria infection. Cell. Microbiol. *18*, 1739–1750.

Pérez-Toledo, K., Rojas-Meza, A.P., Mancio-Silva, L., Hernández-Cuevas, N.A., Delgadillo, D.M., Vargas, M., Martínez-Calvillo, S., Scherf, A., and Hernandez-Rivas, R. (2009). *Plasmodium falciparum* heterochromatin protein 1 binds to tri-methylated histone 3 lysine 9 and is linked to mutually exclusive expression of var genes. Nucleic Acids Res. *37*, 2596–2606.

Ponnudurai, T., Lensen, A.H., Van Gemert, G.J., Bensink, M.P., Bolmer, M., and Meuwissen, J.H. (1989). Infectivity of cultured *Plasmodium falciparum* gametocytes to mosquitoes. Parasitology *98*, 165–173.

Prudêncio, M., and Mota, M.M. (2007). To migrate or to invade: those are the options. Cell Host Microbe *2*, 286–288.

Quinlan, A.R., and Hall, I.M. (2010). BEDTools: a flexible suite of utilities for comparing genomic features. Bioinformatics *26*, 841–842.

Ralph, S.A., Bischoff, E., Mattei, D., Sismeiro, O., Dillies, M.A., Guigon, G., Coppee, J.Y., David, P.H., and Scherf, A. (2005). Transcriptome analysis of antigenic variation in *Plasmodium falciparum - var* silencing is not dependent on antisense RNA. Genome Biol. *6*, R93.

Ramírez, F., Ryan, D.P., Grüning, B., Bhardwaj, V., Kilpert, F., Richter, A.S., Heyne, S., Dündar, F., and Manke, T. (2016). deepTools2: a next generation web server for deep-sequencing data analysis. Nucleic Acids Res. *44* (*W1*), W160–W165.

Rénia, L., Mattei, D., Goma, J., Pied, S., Dubois, P., Miltgen, F., Nüssler, A., Matile, H., Menégaux, F., Gentilini, M., et al. (1990). A malaria heat-shock-like determinant expressed on the infected hepatocyte surface is the target of antibody-dependent cell-mediated cytotoxic mechanisms by nonparenchymal liver cells. Eur. J. Immunol. *20*, 1445–1449.

Richie, T.L., Billingsley, P.F., Sim, B.K., James, E.R., Chakravarty, S., Epstein, J.E., Lyke, K.E., Mordmüller, B., Alonso, P., Duffy, P.E., et al. (2015). Progress with *Plasmodium falciparum* sporozoite (PfSPZ)-based malaria vaccines. Vaccine *33*, 7452–7461.

Ritchie, M.E., Phipson, B., Wu, D., Hu, Y., Law, C.W., Shi, W., and Smyth, G.K. (2015). limma powers differential expression analyses for RNA-sequencing and microarray studies. Nucleic Acids Res. *43*, e47.

Robinson, M.D., McCarthy, D.J., and Smyth, G.K. (2010). edgeR: a Bioconductor package for differential expression analysis of digital gene expression data. Bioinformatics *26*, 139–140.

Robinson, J.T., Thorvaldsdóttir, H., Winckler, W., Guttman, M., Lander, E.S., Getz, G., and Mesirov, J.P. (2011). Integrative genomics viewer. Nat. Biotechnol. *29*, 24–26.

Roestenberg, M., McCall, M., Hopman, J., Wiersma, J., Luty, A.J., van Gemert, G.J., van de Vegte-Bolmer, M., van Schaijk, B., Teelen, K., Arens, T., et al. (2009). Protection against a malaria challenge by sporozoite inoculation. N. Engl. J. Med. *361*, 468–477.

Rovira-Graells, N., Gupta, A.P., Planet, E., Crowley, V.M., Mok, S., Ribas de Pouplana, L., Preiser, P.R., Bozdech, Z., and Cortés, A. (2012). Transcriptional variation in the malaria parasite *Plasmodium falciparum*. Genome Res. *22*, 925–938.

Schats, R., Bijker, E.M., van Gemert, G.J., Graumans, W., van de Vegte-Bolmer, M., van Lieshout, L., Haks, M.C., Hermsen, C.C., Scholzen, A., Visser, L.G., and Sauerwein, R.W. (2015). Heterologous protection against malaria after immunization with *Plasmodium falciparum* sporozoites. PLoS ONE *10*, e0124243.

Smith, J.D. (2014). The role of PfEMP1 adhesion domain classification in *Plasmodium falciparum* pathogenesis research. Mol. Biochem. Parasitol. *195*, 82–87.

Smith, J.D., Rowe, J.A., Higgins, M.K., and Lavstsen, T. (2013). Malaria's deadly grip: cytoadhesion of *Plasmodium falciparum*-infected erythrocytes. Cell. Microbiol. *15*, 1976–1983.

Teirlinck, A.C., Roestenberg, M., van de Vegte-Bolmer, M., Scholzen, A., Heinrichs, M.J., Siebelink-Stoter, R., Graumans, W., van Gemert, G.J., Teelen, K., Vos, M.W., et al. (2013). NF135.C10: a new *Plasmodium falciparum* clone for controlled human malaria infections. J. Infect. Dis. *207*, 656–660.

Thorvaldsdóttir, H., Robinson, J.T., and Mesirov, J.P. (2013). Integrative Genomics Viewer (IGV): high-performance genomics data visualization and exploration. Brief. Bioinform. *14*, 178–192.

Wahlgren, M., Goel, S., and Akhouri, R.R. (2017). Variant surface antigens of *Plasmodium falciparum* and their roles in severe malaria. Nat. Rev. Microbiol. *15*, 479–491.

World Health Organization (2017). Fact sheet: world malaria report 2017. http://www.who.int/mediacentre/factsheets/fs094/en/.

Zhang, Y., Liu, T., Meyer, C.A., Eeckhoute, J., Johnson, D.S., Bernstein, B.E., Nusbaum, C., Myers, R.M., Brown, M., Li, W., and Liu, X.S. (2008). Model-based analysis of ChIP-seq (MACS). Genome Biol. *9*, R137.

Cell Reports, Volume *22*

Supplemental Information

A Specific PfEMP1 Is Expressed in *P. falciparum* Sporozoites and Plays a Role in Hepatocyte Infection

Gigliola Zanghì, Shruthi S. Vembar, Sebastian Baumgarten, Shuai Ding, Julien Guizetti, Jessica M. Bryant, Denise Mattei, Anja T.R. Jensen, Laurent Rénia, Yun Shan Goh, Robert Sauerwein, Cornelus C. Hermsen, Jean-François Franetich, Mallaury Bordessoulles, Olivier Silvie, Valérie Soulard, Olivier Scatton, Patty Chen, Salah Mecheri, Dominique Mazier, and Artur Scherf

SUPPLEMENTARY FIGURE & LEGENDS :

Figure S1:

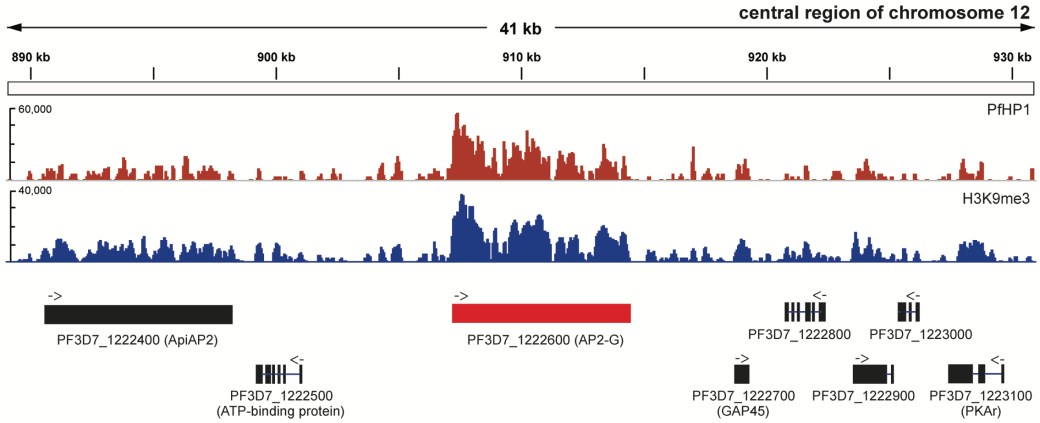

Figure S1. Related to Figure 2. H3K9me3 and PfHP1 are enriched at the AP2-G genomic locus on chromosome 12 in sporozoites. ChIP-seq analysis shows the enrichment of PfHP1 (red) and H3K9me3 (blue) at the AP2-G locus (highlighted in red), with genomic position indicated at the top in kilobases. Coverage plots are represented as average reads per million reads mapped (RPM) over bins of 1 nucleotide with the maximum value of y-axis indicated. Data are representative of three or more independent experiments.

Figure S2:

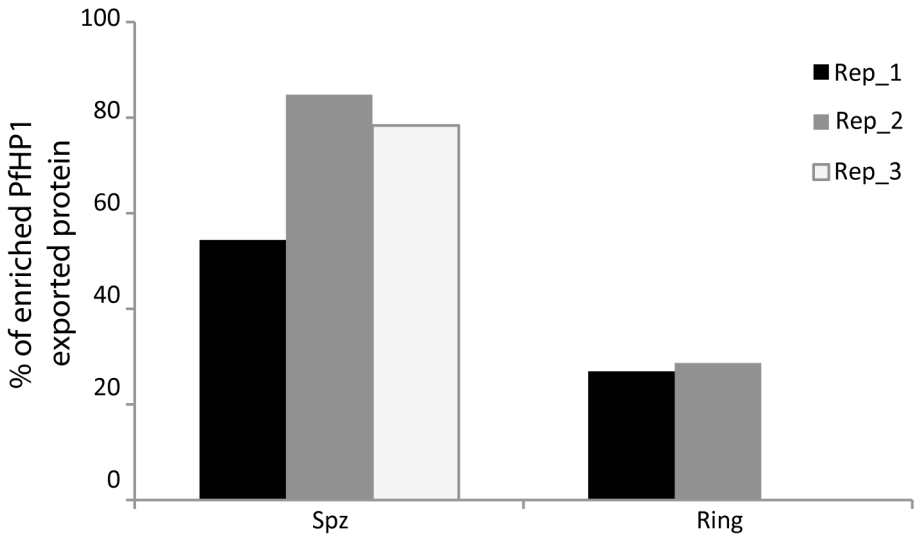

Figure S2. Related to Figure 3. Comparison of PfHP1 enrichment in genes encoding exported proteins in sporozoites and asexual ring stage parasites. The percentage of genes encoding erythrocyte stage exported proteins (containing a PEXEL motif) with PfHP1 enrichment in three biological replicates of sporozoites is increased when compared to asexual blood stage parasites (two biological replicates). Rep 1=Pilot, Rep 2=L1 and Rep 3=L3 for the sporozoite samples and Rep 1=A and Rep2 =B for the asexual blood stage samples (Refer to Supplementary Table S6).

Figure S3:

A

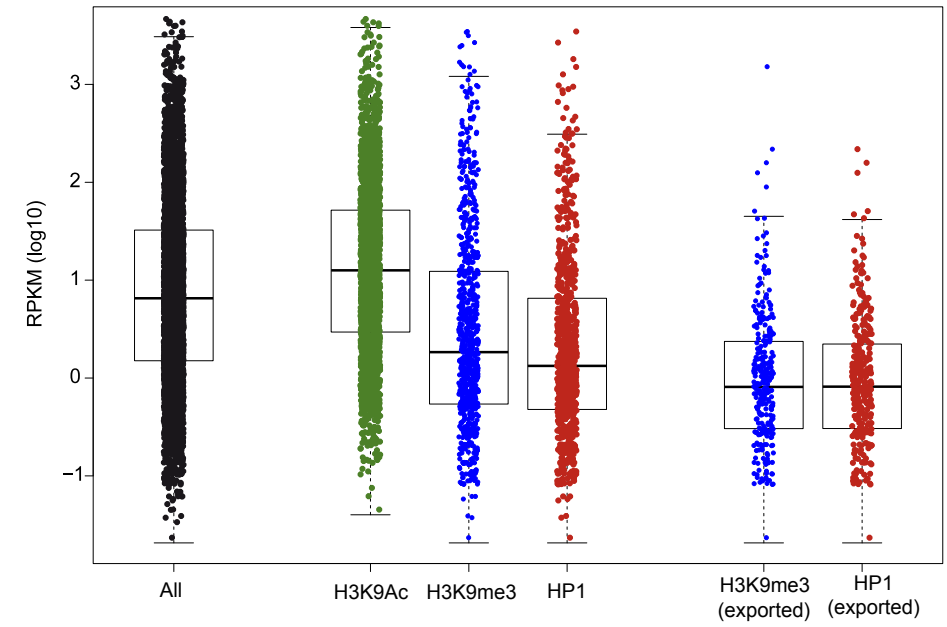

B

	H3K9Ac	H3K9me3	HP1
Total peaks	4620	1572	1606
peaks in genes (# unique genes)	3773 (2612)	1322 (945)	1210 (904)
Transcription Level			
High	846	146	88
Medium	741	111	103
Moderate	580	164	171
Low	377	403	429

Figure S3 Related to Figure 3 and Figure 4. Correlation of PfHP1 and H3K9me3 occupancy within gene bodies to transcriptional levels in sporozoite stages. A) Distribution of steady state mRNA levels (y-axis; calculated as $\log_{10}$RPKM (reads per kilobase of exon model per one million mapped reads); Refer to Supplementary Table S3) of all *P. falciparum* genes (in black) is compared to genes enriched with either H3K9Ac (green), H3K9me3 (blue) or PfHP1 (red) in sporozoites. The presence of H3K9Ac leads to overall higher transcription, whereas the presence of H3K9me3 and PfHP1 leads to transcriptional repression. Genes encoding proteins that are predicted to be exported to the RBC surface

during the blood stages (and containing a PEXEL motif) show low to zero transcription in sporozoites. **B**) Top: A summary of H3K9Ac, H3K9me3 and PfHP1 peaks within genes, as determined by MACS2 peak calling analysis (Refer to Supplementary Table S2). Bottom: Steady state mRNA levels of all genes were sorted into four equally sized groups in decreasing order of magnitude of expression (*i.e.*, RPKM) and analyzed for the occupancy of the different epigenetic marks. In general, genes associated with H3K9Ac have higher steady state mRNA levels as compared to genes associated with either PfHP1 or H3K9me3.

Figure S4:

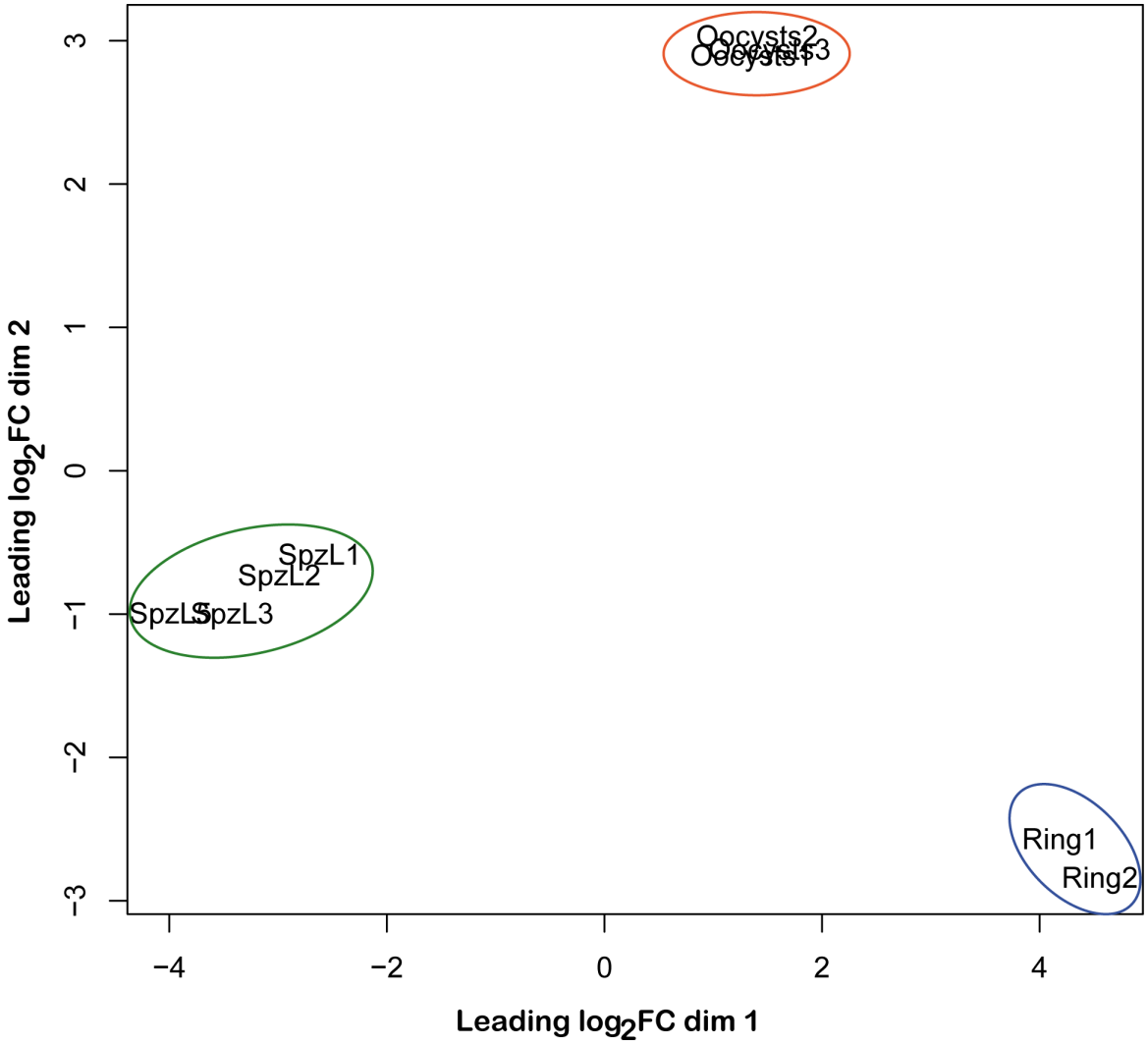

Figure S4. Related to Figure 4. Similarity of the transcriptomes of the different life cycle stages of *P. falciparum* analyzed in this study. A multidimensional scaling plot representing each RNA-seq dataset in two dimensions, such that the distances between each dataset reflect the typical $\log_2$(fold change) ($\log_2$FC) between them. The clustering of similar datasets is highlighted to emphasize the separation of samples into natural groups, based on life cycle stage. See Supplementary Table S3 for more details.

Figure S5:

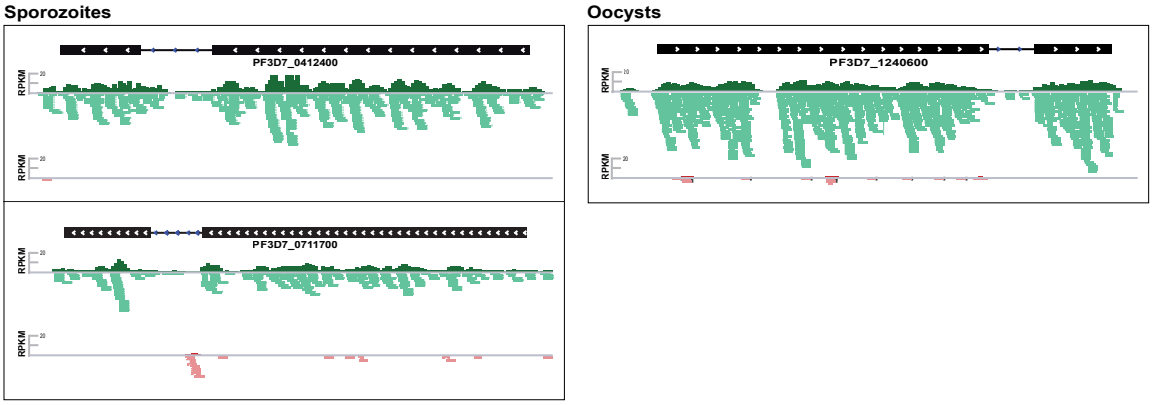

Figure S5. Related to figure 4. Coverage plot of *var* gene expression analyzed by RNA-seq. Top: Transcriptional levels are indicated as RPKM, *i.e.*, reads per kilobase of exon per one million mapped reads, Bottom: mapped reeds. For sense RNA (light green) and antisense RNA (red). See Supplementary Table S4 for more details

Figure S6:

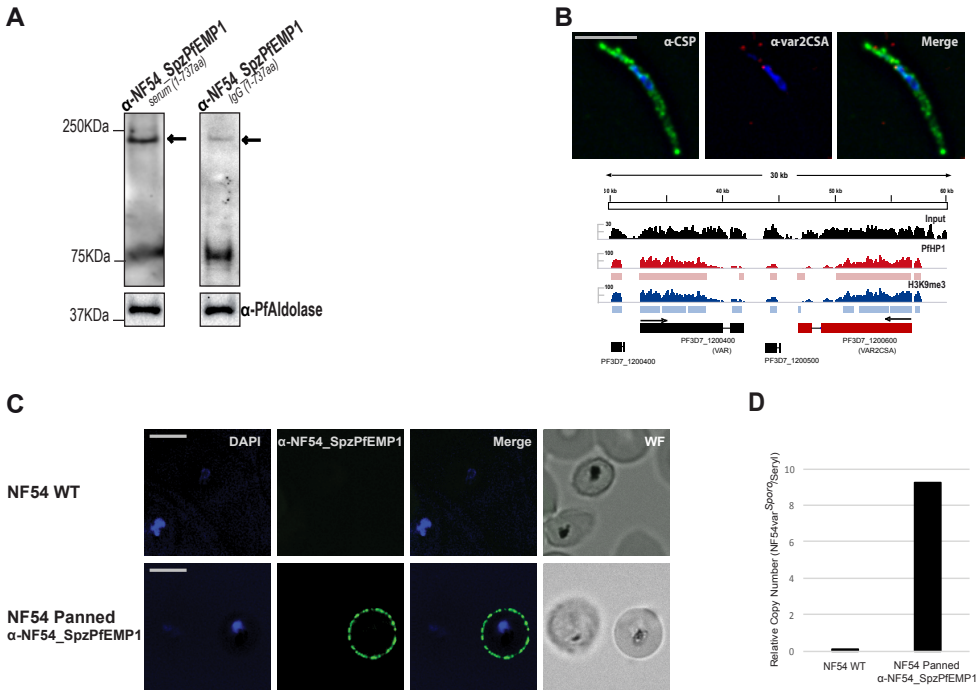

Figure S6. Related to Figure 5. Immunofluorescence analysis of PfEMP1 protein expression in sporozoites and infected red blood cells (iRBCs). (**A**) Western blot analysis of sporozoite extracts using anti-NF54_SpzPfEMP1 antibodies. Anti-PfAldolase antibodies served as a positive control for protein extraction. Molecular weights are shown at the left of the blot and PfEMP1 is indicated with an arrow. (**B**) Top: Immunofluorescence analysis of fixed and permeabilized sporozoites using anti-var2CSA (red) and anti-CSP (green) antibodies. Bottom: Coverage plot (average RPM over bins of 1 nucleotide) representing the enrichment levels of PfHP1 and H3K9me3 at the *var2CSA* locus. The genomic position is indicated at the top in kb. For all panels, DNA was stained with DAPI (blue), indicating the nucleus, and the scale bar is 5 µm. (**C**) Surface immunofluorescence of living iRBCs at 30 hours post infection using anti-NF54_SpzPfEMP1 1/1000 dilution (green). Top panel shows WT NF54 trophozoites and lower panel panned NF54 parasites. DNA was stained with DAPI (blue) and the wide-field (WF) image is shown at the right. Scale bar = 5 µm. (**D**) RT-qPCR analysis of the WT NF54 and antibody NF54_SpzPfEMP1-panned NF54 parasites. RNA transcripts from highly synchronized ring stage parasites 12 hours post-infection. *var* gene cDNA levels (NF54*var*^{sporo}) are normalized to those of seryl tRNA synthetase.